CrossMark

Thermokinetic analysis of the stability of malic and salicylic acids in cosmeceutical formulations containing metal oxides

An-Chi Huang[1] · Yu-Kai Chuang[2] · Chung-Fu Huang[1] · Chi-Min Shu[1,2,3] (iD)

Abstract

Cosmeceutical products that contain malic acid (MA), salicylic acid (SA), and hyaluronic acid as well as a variety of antioxidants are used worldwide. Therefore, safer ingredients of cosmeceutical products have become an important issue based on sales volume. In general, the chemical composition may affect the thermal stability of a cosmeceutical product. Temperature changes may occur in the manufacturing, storage, and transport of the product, affecting its stability. Because cosmeceutical products are placed directly on the skin, sensitivity has become an increasing concern. However, potential risks have not been clearly identified. To investigate the thermal stability behavior of regular cosmeceutical materials, thermogravimetry and differential scanning calorimetry have been used. For this study, the thermal stability of MA and SA was studied, and the acids were individually mixed with CuO or Fe_2O_3 to evaluate the effect of adding metal oxides. According to the DSC curves, the apparent exothermic onset temperature occurred when MA and SA were mixed with Fe_2O_3. Apparent activation energy values of individual samples calculated using the ASTM E698 and Ozawa–Flynn–Wall methods ranged from 72.2 to 87.4 kJ mol^{-1} and from 84.2 to 98.7 kJ mol^{-1}, respectively. The results can be used to calculate the optimal parameters for safe cosmeceutical manufacturing and establishing a database of MA and SA for loss prevention protocols.

List of symbols

A	Frequency factor (s^{-1})
D	Correction coefficient for apparent activation energy (dimensionless)
E_a	Apparent activation energy (kJ mol^{-1})
K	Reaction rate constant (min^{-1})
R	Gas constant (8.314 J mol^{-1} K)
T_0	Apparent exothermic onset temperature (°C)
T_p	Peak temperature (°C)
α	Conversion degree (dimensionless)
β	Heating rate (°C min^{-1})
ΔH_d	Heat of decomposition (J g^{-1})

✉ Chi-Min Shu
shucm@yuntech.edu.tw

1   Graduate School of Engineering Science and Technology, National Yunlin University of Science and Technology (YunTech), Yunlin 64002, Taiwan, ROC

2   Department of Safety, Health, and Environmental Engineering, YunTech, Yunlin 64002, Taiwan, ROC

3   Center for Process Safety and Industrial Disaster Prevention, YunTech, Yunlin 64002, Taiwan, ROC

Introduction

Malic acid (MA), a component in various common foods, is a mild and relatively harmless acid when used in appropriate amounts. This acid is used not only as a food supplement, but also as a common additive in skin care products because of its established exfoliating properties. Some products containing MA include hair conditioners, facial moisturizers, shampoos, nail products, and antiaging treatments. One of its purposes is to adjust the acid–base balance or pH of these products to ensure their optimal function. Due to its chemical composition, it is able to penetrate the skin deeply by reducing Ca^{2+} from surface of skin. As a result, cosmeceutical products that contain this supplement can greatly help in improving skin smoothness and complexion pigmentation. One of the greatest attributes of MA, as both a food supplement and a skincare agent, is that it is a completely natural organic compound [1]. MA can soften cuticles, remove rough aging skin, and increase collagen as well as elastic fiber protein production. It also has a whitening effect and antioxidant capacity and is commonly extracted from apples. Also known as alpha

hydroxyl acid, it primarily functions because of its irritant property that helps the body exfoliate the top layer of skin cells [2].

Salicylic acid (SA), a white odorless crystalline powder, occurs naturally in willow bark, white birch leaves, and sweet birch bark. SA has an excellent ability for exfoliating and cleaning pores, as well as removing excessive keratin in hyperkeratotic skin disorders. SA is safe, and its skin irritation is lower than that of MA. Therefore, it has therefore recently become a common component of skincare products. When applied on the facial skin, SA helps the skin shed dead cells from the outer layer and decreases swelling and redness. SA reduces pimples and improves healing. Like other hydroxyl acids, SA is a key component in many skin care products for the treatment of corns, acne, seborrheic dermatitis, ichthyosis, keratosis pilaris, calluses, and warts [3, 4]. SA is a beta hydroxyl acid that is either found naturally or synthetically produced for skin treatment products. The major advantage of SA is its ability to expel skin cells of the most outer layer, the stratum corneum. This keratolytic effect depends on the concentration of SA used in a cream product [5].

In cosmeceutical products, numerous mineral materials are added. Therefore, the thermal behavior of metal ions mixed with MA and SA is worth analyzing. Mixing different materials with metal oxides may entail unknown risks [6, 7]. The thermal stability of MA, SA, and samples mixed with CuO or Fe_2O_3 has been determined. Thermogravimetry (TG) has been used to obtain the values of safety parameters and thermal stability, such as the mass loss, mass loss derivative, initial mass loss temperature, highest mass loss rate temperature, and mass loss rate slowdown temperature [8, 9]. Differential scanning calorimetry (DSC) can determine preliminary thermokinetic parameters. Heat flow is used to ascertain kinetic parameters, such as T_0, T_p, and ΔH_d. DSC is widely employed to characterize thermally activated processes that occur in materials during a defined decomposition period involving a change in temperature [10, 11]. Our aim was to confirm the thermokinetic properties of cosmeceutical products and accordingly reduce the risk of thermal hazards from the usage, storage, and transport of cosmeceuticals products as much as possible.

Experiments and methods

Materials

The structures of MA and SA are shown in Figs. 1 and 2. MA (95.0 mass%) was purchased from Sigma-Aldrich
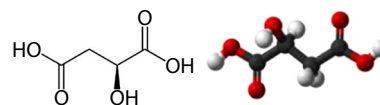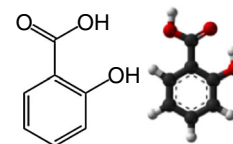

Fig. 1 Structure of MA

Fig. 2 Structure of SA

(Saint Louis, Missouri, USA). SA was purchased from Avantor Performance Materials, Inc. (Center Valley, Pennsylvania, USA). To test the thermal behavior of MA and SA mixed with mineral materials, we acquired CuO and Fe_2O_3 from Showa Kako Corporation (Osaka, Japan). The hydroxyl acid and mineral samples were used as powders to ensure an even mixture of the samples tested. The samples were stored in an electronic cabinet at 25.0 °C. The relative humidity of the electronic cabinet was constantly kept at 45.0%.

Thermogravimetry

TG was performed using a PerkinElmer Pyris 1 thermogravimeter (Waltham, Massachusetts, USA). TG has a powerful separating feature; the mass of the sample is monitored relative to time while the temperature of the sample in the designated atmosphere is varied. This technique is used to determine material compositions [12, 13]. We used it to test the mass loss and thermal stability parameters of MA, SA, and mixtures of an individual acid with metal oxides. TG is primarily used in research on temperature-induced changes in chemicals to verify whether the materials or chemicals experience a reduction in mass and to determine the thermal characteristics and compositions of the sample chemicals. The temperature range in this study was adjusted from 30.0 to 300.0 °C, and the heating rate was set to 0.5, 1.0, 2.0, 4.0, or 8.0 °C min^{-1}. The experimental atmosphere was ambient air, and the flow rate was 20.0 mL min^{-1} [14, 15]. Each set of experiments was replicated at least thrice to confirm the authenticity of samples used in the TG tests.

Differential scanning calorimetry

For heat flow experiments, we employed DSC 821^e of a Mettler TA8000 system (Greifensee, Switzerland) with a nitrogen gas atmosphere. DSC uses a sample and a reference substance kept in separate chambers. Each chamber is heated by a separate source so that their temperatures are

always equal. This is accomplished using thermocouples; the temperature of each chamber is frequently monitored, and if a temperature difference is detected, then heat is added to the cooling chamber to compensate for the discrepancy. The heating rate used to preserve equivalent temperatures is recorded as a function of the temperature. This instrument can be used to establish basic thermokinetic parameters. The DSC instrument used in this study was calibrated for a heating rate of 4.0 °C min^{-1}.

All experimental samples were placed in a sealed high-pressure plated crucible that can sustain temperatures up to 720.0 °C [16]. The system was tested to operate under pressures of 100.0 bar. DSC is a highly reliable thermo-analytical technique for collecting thermokinetic data [17, 18]. DSC experiments can demonstrate the differences in the amount of heat required to maintain the temperature of microvolume samples, mainly through heat flow. Approximately 3.5 ± 0.5 mg of the samples was used to acquire the experimental data. The thermal heating rates were set to 0.5, 1.0, 2.0, 4.0, and 8.0 °C min^{-1}. The temperature range was 30.0 to 400.0 °C. Each sample was tested thrice for reproducibility to reconfirm the authenticity of the experimental results.

Results and discussion

TG analysis of MA, SA, and mixtures of an individual acid with CuO or Fe$_2$O$_3$ was performed. To determine the various characteristic temperatures of these samples for different decomposition behaviors, samples were tested through TG at heating rates of 0.5, 1.0, 2.0, 4.0, and 8.0 °C min^{-1}. Figures 3 and 4 show the mass loss curves of MA and SA, indicating that they had a similar decomposition process and thermogravimetric loss. The thermogravimetric curves showed that the mass loss of the two samples in
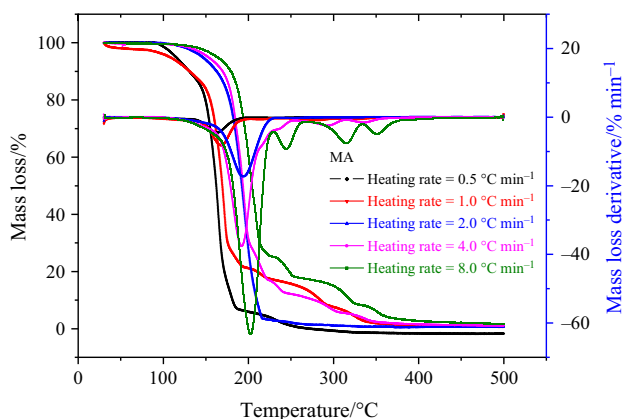
the heating environment was only pure thermal decomposition, and as the heating rate increased, there was a delay in the mass loss.

Figures 5–8 show the decomposition phenomena of MA and SA mixed with CuO or Fe$_2$O$_3$ analyzed through TG at heating rates of 0.5, 1.0, 2.0, 4.0, and 8.0 °C min^{-1}. The figures clearly illustrate that the final mass loss was approximately 45.0–55.0% for MA and SA when metal oxides were added. For MA mixed with CuO or Fe$_2$O$_3$, the first step of thermal decomposition occurred in the 30.0–150.0 °C temperature range, and the mass loss was approximately 10.0%. The second step of the thermal decomposition occurred from 150.0 to 250.0 °C and from 150.0 to 300.0 °C. The mass loss of MA mixed with CuO was more moderate than that of MA mixed with Fe$_2$O$_3$, and the final mass loss was approximately 40.0%.

For SA mixed with CuO or Fe$_2$O$_3$, the first step occurred in the 30.0–120.0 °C range, which is lower than that for MA mixed with metal oxides. For both samples, rapid

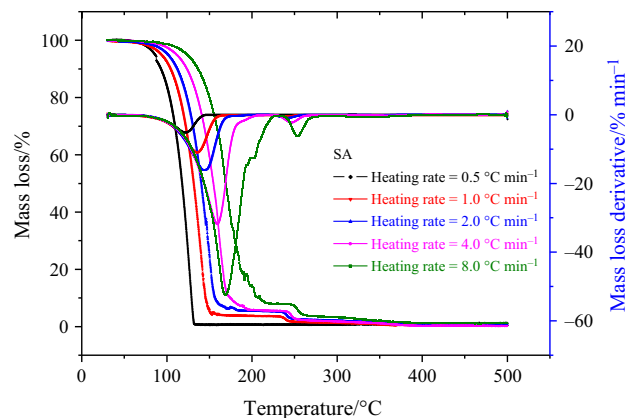**Fig. 4** Plots of mass loss and mass loss derivative versus temperature for SA at heating rates of 0.5, 1.0, 2.0, 4.0, and 8.0 °C min^{-1} in TG tests

Fig. 3 Plots of mass loss and mass loss derivative versus temperature for MA at heating rates of 0.5, 1.0, 2.0, 4.0, and 8.0 °C min^{-1} in TG tests
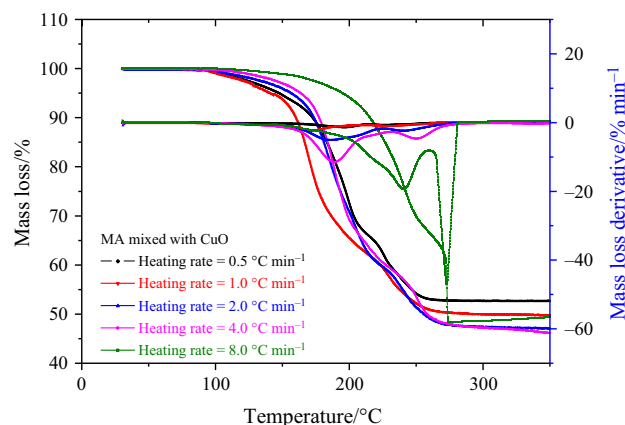
Fig. 5 Plots of mass loss and mass loss derivative versus temperature for MA mixed with CuO at heating rates of 0.5, 1.0, 2.0, 4.0, and 8.0 °C min^{-1} in TG tests
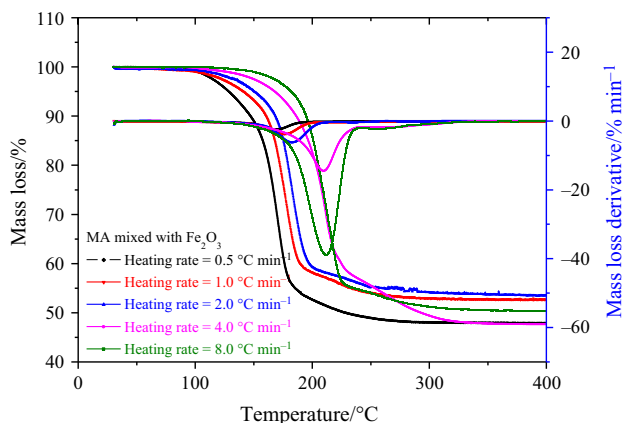
Fig. 6 Plots of mass loss and mass loss derivative versus temperature for MA mixed with Fe_2O_3 at heating rates of 0.5, 1.0, 2.0, 4.0, and 8.0 °C min^{-1} in TG tests
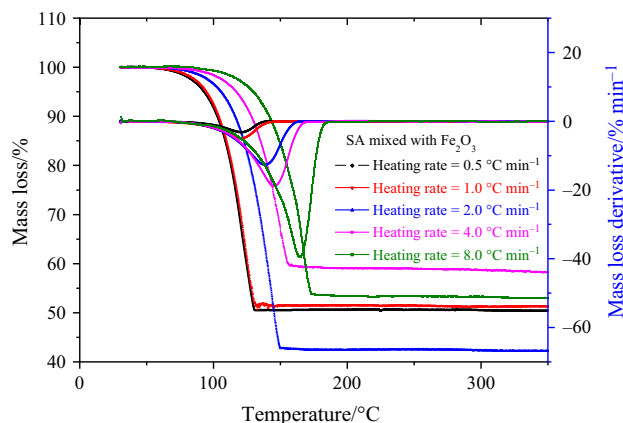

Fig. 8 Plots of mass loss and mass loss derivative versus temperature for SA mixed with Fe_2O_3 at heating rates of 0.5, 1.0, 2.0, 4.0, and 8.0 °C min^{-1} in TG tests
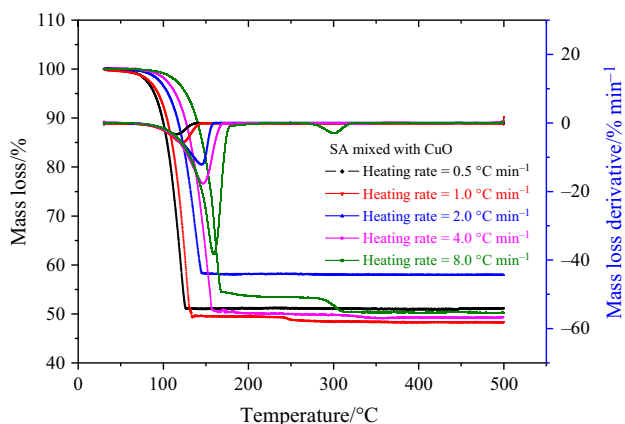

Fig. 7 Plots of mass loss and mass loss derivative versus temperature for SA mixed with CuO at heating rates of 0.5, 1.0, 2.0, 4.0, and 8.0 °C min^{-1} in TG tests

Fig. 9 DSC curves of heat flow versus temperature for MA and MA mixed with metal oxides at heating rate of 4.0 °C min^{-1}

decomposition occurred in the second step, and the final mass loss was approximately 50.0%. The final mass loss of MA or SA mixed with CuO or Fe_2O_3 was approximately 40.0% and was due to the addition of the metal oxide. The melting points of CuO and Fe_2O_3 are 1201.0 and 1566.0 °C, respectively.

DSC tests of MA, SA, and mixtures of an individual acid with CuO or Fe_2O_3 were conducted. Random sampling was used in all experiments to avoid unexpected factors that may cause inaccuracy. Figures 9–14 show the DSC curves of heat flow versus temperature for the decomposition of the materials at heating rates of 0.5, 1.0, 2.0, 4.0, and 8.0 °C min^{-1}. The samples underwent reactions during the heating process. As the heating rate increased, the degradation temperature of the samples became higher, as previously reported [19]. Figures 9–11 show that the reaction time for MA and MA mixed with CuO or Fe_2O_3 increased after decomposition through the
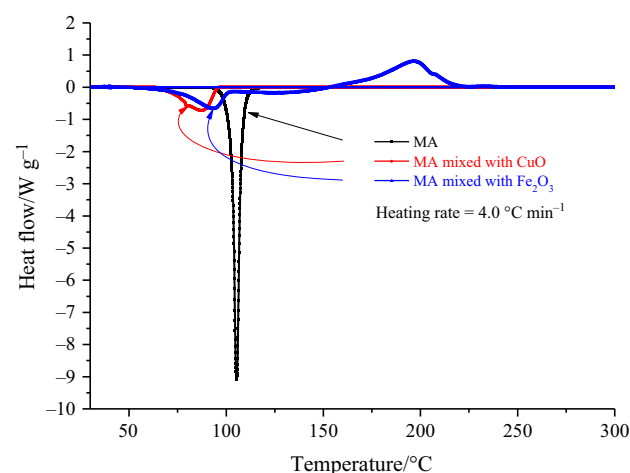
heat accumulation effect, and this increase was accompanied by the release of heat. During the reaction, both MA mixed with CuO and that mixed with Fe_2O_3 at 60.0 °C both underwent a phase inversion involving melting, resulting in an endothermic reaction. An exothermic event occurred between 100.0 and 150.0 °C with continued thermal decomposition. Here, the phase transition process was required to absorb the heat generated, and the heat consumed by the endothermic reaction led to a decrease in heat flow. The thermal decomposition reaction of MA mixed with CuO or Fe_2O_3 continued to be exothermic. The second exothermic peaks of MA mixed with CuO or Fe_2O_3 occurred between approximately 100.0–150.0 and 150.0–250.0 °C and dominated the most intense temperature range. The test data are listed in Tables 1 and 2. Moreover, ΔH_d obtained from the samples was measured in the exothermic peak area. Because heat absorption and heat

Table 1 Thermal stability data from nonisothermal heating experiments for MA mixed with CuO at heating rates of 0.5, 1.0, 2.0, 4.0, and 8.0 °C min^{-1}

| MA + CuO		Endothermic		Exothermic		
β/°C min^{-1}	Mass/mg	T_0/°C	T_p/°C	T_0/°C	T_p/°C	ΔH_d/J g^{-1}
0.5	3.4	96.15	96.33	99.91	99.98	11.13
1.0	3.5	98.18	98.27	102.42	102.42	30.80
2.0	3.1	50.02	102.15	102.59	104.28	30.33
4.0	3.3	87.69	104.15	107.02	113.40	65.52
8.0	3.1	43.61	105.32	110.05	125.31	47.55

Table 2 Thermal stability data from nonisothermal heating experiments for MA mixed with Fe$_2$O$_3$ at heating rates of 0.5, 1.0, 2.0, 4.0, and 8.0 °C min^{-1}

MA + Fe$_2$O$_3$		Endothermic		Exothermic		
β/°C min^{-1}	Mass/mg	T_0/°C	T_p/ C	T_0/°C	T_p/°C	ΔH_d/J g^{-1}
0.5	3.5	81.77	94.0	97.63	161.16	172.25
1.0	3.4	72.22	91.73	100.40	173.90	179.38
2.0	3.0	78.45	91.07	134.42	187.96	168.90
4.0	3.0	63.44	93.54	177.34	196.43	174.68
8.0	3.2	54.17	99.37	127.99	209.50	289.49

generation occurred successively, the integral of heat generation was calculated from the baseline, at which the heat flow was 0 W g^{-1}. Additionally, the T_0 of the endothermic and exothermic phases was determined as the intersection point of the DSC curve and the baseline, as shown in Figs. 10–14.

The DSC heating curves for heating rates of 0.5, 1.0, 2.0, 4.0, and 8.0 °C min^{-1} in Figs. 12–14 show the reaction behavior of SA and SA mixed with CuO or Fe$_2$O$_3$. The difference from MA mixed with CuO or Fe$_2$O$_3$ is that the endothermic phenomenon was faster and more intense. During the reaction, a phase inversion occurred at approximately 150.0 °C, which is much higher than the temperature of 60.0 °C for the endothermic reaction of MA mixed with CuO or Fe$_2$O$_3$. As the temperature increased to 160.0 °C, an exothermic reaction was initiated. The test sample data, presented in Tables 3 and 4, show that the addition of CuO or Fe$_2$O$_3$ in a solid state to SA produces melting during the heating process, and the sample changes from solid to liquid. The second exothermic peaks occurred between 150.0 and 200.0 °C and between 160.0 and 260.0 °C. The exothermic period of SA mixed with CuO was shorter and more intense than that of SA mixed with Fe$_2$O$_3$.

Five heating rates and baseline curves were employed as prerequisites for thermal analysis [20], and kinetic results were obtained using the ASTM E698 method to calculate the apparent activation energy (E_a) [21, 22]. E_a is the minimum energy required for a chemical reaction to occur.
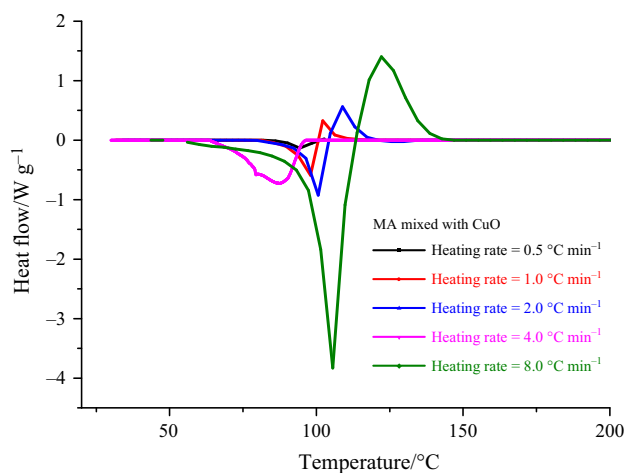
Fig. 10 DSC curves of temperature versus heat flow for MA mixed with CuO at heating rates of 0.5, 1.0, 2.0, 4.0, and 8.0 °C min^{-1}

For a complex chemical reaction, the conversion, time, or environmental temperature can affect E_a. The linear regression relationship between the conversion rate and the heating rates, obtained using the ASTM E698 method, is shown in Eqs. (1) to (3) and can be used to determine E_a (α):

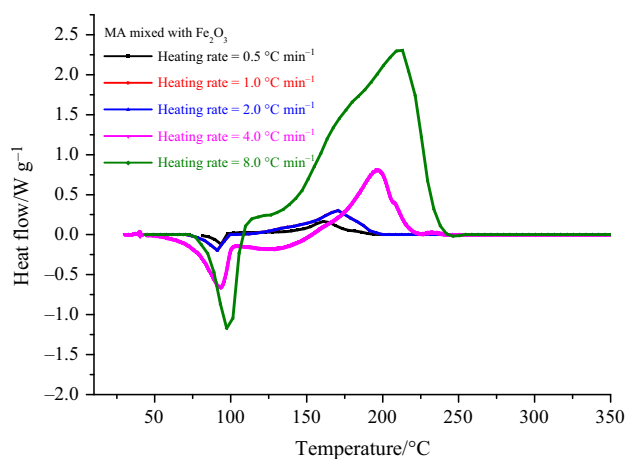$$E_a = \left(\frac{-2.303R}{D}\right)\left[\frac{d(\log_{10}\beta)}{d(1/T_p)}\right] \tag{1}$$

Fig. 11 DSC curves of temperature versus heat flow for MA mixed with Fe$_2$O$_3$ at heating rates of 0.5, 1.0, 2.0, 4.0, and 8.0 °C min^{-1}

Fig. 12 DSC curves of heat flow versus temperature for SA and SA mixed with metal oxides at heating rate of 4.0 °C min^{-1}
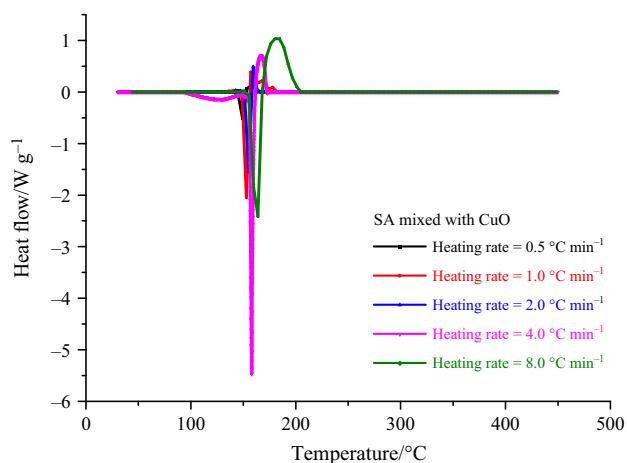
Fig. 13 DSC curves of temperature versus heat flow for SA mixed with CuO at heating rates of 0.5, 1.0, 2.0, 4.0, and 8.0 °C min^{-1}
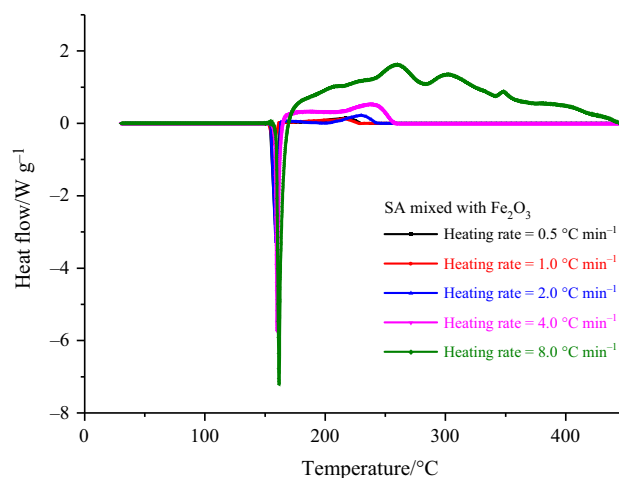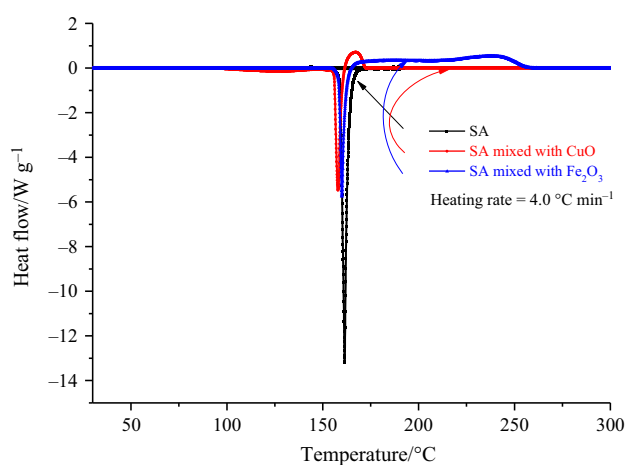

Fig. 14 DSC curves of temperature versus heat flow for SA mixed with Fe$_2$O$_3$ at heating rates of 0.5, 1.0, 2.0, 4.0, and 8.0 °C min^{-1}

Fig. 15 E_a analysis graphs for MA mixed with Fe$_2$O$_3$ at heating rates of 0.5, 1.0, 2.0, 4.0, and 8.0 °C min^{-1} plotted using ASTM E698 method

Fig. 16 E_a analysis graphs for SA and SA mixed with CuO or Fe$_2$O$_3$ at heating rates of 0.5, 1.0, 2.0, 4.0, and 8.0 °C min^{-1} plotted using ASTM E698 method

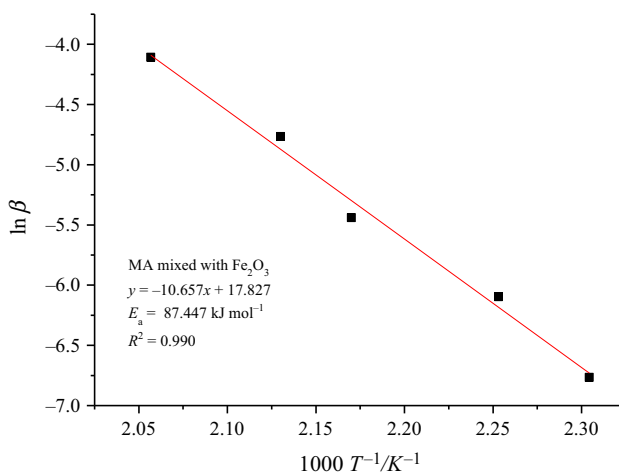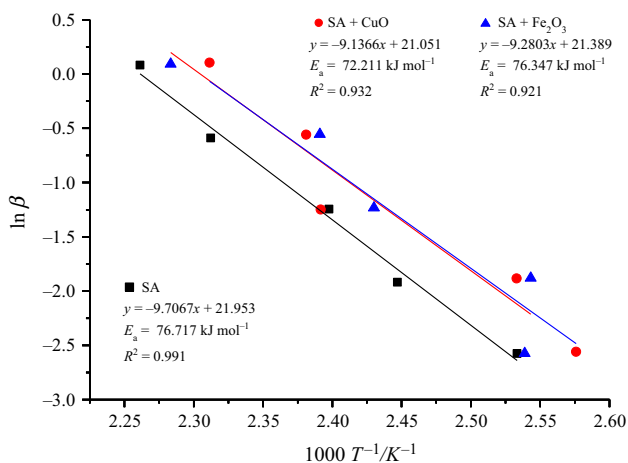**Table 3** Thermal stability data from nonisothermal heating experiments for SA mixed with CuO at heating rates of 0.5, 1.0, 2.0, 4.0, and 8.0 °C min^{-1}

SA + CuO		Endothermic		Exothermic		
β/°C min^{-1}	Mass/mg	T_0/°C	T_p/°C	T_0/°C	T_p/°C	ΔH_d/J g^{-1}
0.5	3.4	140.95	149.32	153.50	161.87	35.42
1.0	3.2	151.09	152.77	154.14	158.10	68.74
2.0	3.5	155.86	158.89	159.94	160.32	68.74
4.0	3.4	92.02	157.78	161.80	167.61	19.38
8.0	3.3	138.33	160.85	163.16	178.63	51.48

Table 4 Thermal stability data from nonisothermal heating experiments for SA mixed with Fe$_2$O$_3$ at heating rates of 0.5, 1.0, 2.0, 4.0, and 8.0 °C min^{-1}

SA + Fe$_2$O$_3$		Endothermic		Exothermic		
β/°C min^{-1}	Mass/mg	T_0/°C	T_p/°C	T_0/°C	T_p/°C	ΔH_d/J g^{-1}
0.5	3.4	157.67	158.56	162.68	216.85	86.39
1.0	3.2	144.70	203.26	161.43	215.81	80.27
2.0	3.2	143.78	158.95	171.43	229.76	87.14
4.0	3.5	158.37	159.78	170.40	238.86	105.07
8.0	3.3	155.92	161.14	169.33	259.20	296.29

$$D = -\frac{d\ln[\rho(x)]}{dx} = -\frac{\left[d\ln(x+2)^{-1}(x)^{-1}\exp(-x)\right]}{dx} \quad (2)$$

$$A = \frac{E_a\beta}{RT_p^2}\exp\left(\frac{E_a}{T_p}\right) \quad (3)$$

Through the linear regression, five heating rates and corresponding peak temperatures were examined. Figures 15 and 16 show a diagram developed using ASTM E698; T_p from each heating rate was used in a non-isothermal experiment with five data sets analyzed using linear regression. Finally, the slopes of the linear regressions of the five heating rates were used to calculate E_a for MA mixed with Fe$_2$O$_3$, SA, SA mixed with CuO, and SA mixed with Fe$_2$O$_3$. The values are approximately 87.4, 76.7, 72.2, and 76.3 kJ mol^{-1}, respectively, as shown in Figs. 15 and 16.

The Ozawa–Flynn–Wall method was adopted to treat the data using integration equations. This fast method is widely used because some intrinsic limitations can be avoided [23, 24]:

$$\ln(\beta_1) + 1.0516\left(\frac{E_a}{RT_{p1}}\right) = \ln(\beta_2) + 1.0516\left(\frac{E_a}{RT_{p2}}\right)$$
$$= \ln(\beta_3) + 1.0516\left(\frac{E_a}{RT_{p3}}\right) = \cdots \quad (4)$$

Briefly, E_a is known as the energy point that a chemical reaction must overcome: the higher the E_a value, the more difficult the reaction will be. The E_a value was calculated using the Ozawa–Flynn–Wall method with different iso-conversion rates according to nonisothermal heating rates for MA or SA mixed with CuO or Fe$_2$O$_3$. Based on the reaction rate results, we compared the different isoconversion rates from 0.99 to 0.01 to obtain the slope and calculate the E_a value of MA or SA mixed with CuO or Fe$_2$O$_3$. Moreover, since decomposition and melting phenomena occurred throughout the DSC experiment, the exothermic process was selected to determine E_a. The reaction rates for five heating rates versus the different isoconversion rates from 0.99 to 0.01 were used to calculate the relationship through linear regression. The results were exceptionally consistent; the slopes were parallel to the reaction rates. The E_a range of MA, SA, and mixtures of an individual acid with CuO or Fe$_2$O$_3$ was from 84.2 to 98.7 kJ mol^{-1}.

Cosmeceutical products that contain both MA and SA are minimally exposed to a low- to medium-temperature environment. However, phenomena that occur in storage and transport processes may lead to hazardous accidents. Therefore, in actual usage conditions, the mentioned processes must still be properly planned and managed. Our results indicated that a minute amount of heat is generated when MA and SA are mixed with Fe$_2$O$_3$ during usage, transport, storage, or disposal.

Conclusions

Our results show that metal oxides such as Fe_2O_3 are catalyst materials for MA and SA. In a low- to medium-temperature environment, adding Fe_2O_3 increased the ΔH_d of MA and SA to 289.49 and 296.29 J g^{-1}, respectively. Adding Fe_2O_3 produces a perceivable exothermic reaction with MA and SA that could endanger people. Fe_2O_3 is a very common substance in the manufacturing of mineral makeup products. When iron reacts with oxygen and moisture exists in the environment, Fe_2O_3 forms in rust. According to our results, the E_a of each sample calculated through ASTM E698 is consistent with the E_a range acquired using the Ozawa–Flynn–Wall method. According to the DSC curves, the exothermic reactions of MA and SA mixed with Fe_2O_3 were greater than those of MA and SA mixed with CuO. Adding Fe_2O_3 to MA and SA not only caused an endothermic reaction initially but also resulted in an exothermic reaction. Therefore, it is essential to choose pipes or receptacles with adequate chemical properties to avoid rust formation. In production processes involving MA and SA, contact with Fe_2O_3, which is commonly used in mineral makeup, must be avoided.

References

1. Telegdi J, Trif L, Nagy E, Mihály J, Molnár N. New comonomers in malic acid polyesters. J Therm Anal Calorim. 2017;129(2):991–1000.
2. Van Staden J, Volschenk H, Van Vuuren H, Viljoen-Bloom M. Malic acid distribution and degradation in grape must during skin contact: the influence of recombinant malo-ethanolic wine yeast strains. S Afr J Enol Vitic. 2017;26(1):16–20.
3. Grimes PE. The safety and efficacy of salicylic acid chemical peels in darker racial–ethnic groups. Dermatol Surg. 1999;25(1):18–22.
4. John J, Devi Rugmini S, Sreedharan Nair B. Kinetic analysis of thermal and hydrolytic decomposition of spiroborate ester of curcumin with salicylic acid. Orient J Chem. 2017;33(2):849–58.
5. Zhou ZZ, Chan HM, Sung HH, Tong HH, Zheng Y. Identification of new cocrystal systems with stoichiometric diversity of salicylic acid using thermal methods. Pharm Res. 2016;33(4):1030–9.
6. do Nascimento ALCS, Teixeira JA, Nunes WDG, Gomes DJC, Gaglieri C, Treu-Filho O, Pivatto M, Caires FJ, Ionashiro M. Thermal behavior of glycolic acid, sodium glycolate and its compounds with some bivalent transition metal ions in the solid state. J Therm Anal Calorim (in press).
7. Tsai YT, You ML, Qian XM, Shu CM. Calorimetric techniques combined with various thermokinetic models to evaluate incompatible hazard of tert-butyl peroxy-2-ethyl hexanoate mixed with metal ions. Ind Eng Chem Res. 2013;52(24):8206–15.
8. Deng J, Zhao JY, Huang AC, Zhang YN, Wang CP, Shu CM. Thermal behavior and microcharacterization analysis of second-oxidized coal. J Therm Anal Calorim. 2017;127(1):439–48.
9. Bisinella RZ, Ribeiro JC, de Oliveira CS, Colman TA, Schnitzler E, Masson ML. Some instrumental methods applied in food chemistry to characterise lactulose and lactobionic acid. Food Chem. 2017;220:295–8.
10. Bezerra GSN, Pereira MAV, Ostrosky EA, Barbosa EG, de Moura MdFV, Ferrari M, Aragão CFS, Gomes APB. Compatibility study between ferulic acid and excipients used in cosmetic formulations by TG/DTG, DSC and FTIR. J Therm Anal Calorim. 2016;127(2):1683–91.
11. Pardauil JJR, de Molfetta FA, Braga M, de Souza LKC, Filho GNR, Zamian JR, da Costa CEF. Characterization, thermal properties and phase transitions of amazonian vegetable oils. J Therm Anal Calorim. 2016;127(2):1221–9.
12. Deng J, Zhao JY, Xiao Y, Zhang YN, Huang AC, Shu CM. Thermal analysis of the pyrolysis and oxidation behaviour of 1/3 coking coal. J Therm Anal Calorim (in press).
13. Tsai YT, Lin SY, Tong JW, Chen WC, Chen WT, Shu CM. Incompatible hazard investigation of a cycloaliphatic epoxy resin using green analytical method. J Therm Anal Calorim. 2015;122(3):1135–41.
14. Tong JW, Chen WC, Tsai YT, Cao Y, Chen JR, Shu CM. Incompatible reaction for (3-4-epoxycyclohexane) methyl-3′-4′-epoxycyclohexyl-carboxylate (EEC) by calorimetric technology and theoretical kinetic model. J Therm Anal Calorim. 2014;116(3):1445–52.
15. Wang CP, Yang Y, Tsai YT, Deng J, Shu CM. Spontaneous combustion in six types of coal by using the simultaneous thermal analysis-Fourier transform infrared spectroscopy technique. J Therm Anal Calorim. 2016;126(3):1591–602.
16. Li KY, Tsai SY, Lin CP, Tsai YT, Shu CM. Smart technology for evaluating fire extinguishing effect of tert-butyl hydroperoxide. Ind Eng Chem Res. 2013;52(32):10969–76.
17. Huang AC, Chen WC, Huang CF, Zhao JY, Deng J, Shu CM. Thermal stability simulations of 1,1-bis(tert-butylperoxy)-3,3,5 trimethylcyclohexane mixed with metal ions. J Therm Anal Calorim. 2017;130(2):949–57.
18. Karl W, Perla R, Gérard C, Franck C, Luc NM, Hayat B, Denis F. Effect of surfactant on structure thermal behavior of cetyl stearyl alcohols. J Therm Anal Calorim. 2015;123(2):1411–7.
19. Kök M. Heating rate effect on the DSC kinetics of oil shales. J Therm Anal Calorim. 2007;90(3):817–21.
20. Tsai LC, Tsai YT, Lin CP, Liu SH, Wu TC, Shu CM. Isothermal versus non-isothermal calorimetric technique to evaluate thermokinetic parameters and thermal hazard of tert-butyl per-oxy-2-ethyl hexanoate. J Therm Anal Calorim. 2012;109(3):1291–6.
21. Das M, Shu CM. A green approach towards adoption of chemical reaction model on 2,5-dimethyl-2,5-di-(tert-butylperoxy)hexane decomposition by differential isoconversional kinetic analysis. J Hazard Mater. 2016;301:222–32.
22. Chen WC, Shu CM. Prediction of thermal hazard for TBPTMH mixed with BPO through DSC and isoconversional kinetics analysis. J Therm Anal Calorim. 2016;126(3):1937–45.
23. Chen WC, Lin JR, Liao MS, Wang YW, Shu CM. Green approach to evaluating the thermal hazard reaction of peracetic acid through various kinetic methods. J Therm Anal Calorim. 2016;127(1):1019–26.
24. Liu SH, Cao CR, Lin YC, Shu CM. Using thermal analysis and kinetic calculation method to assess the thermal stability of 2,2′-azobis-(2-methylbutyronitrile). J Therm Anal Calorim (in press).